Increasing the Rate of Energy Transfer between the LHI Antenna and the Reaction Center in the Photosynthetic Bacterium *Rhodobacter sphaeroides*

Zivile Katiliene, Evaldas Katilius, Gregory H. Uyeda, JoAnn C. Williams, and Neal W. Woodbury*

Department of Chemistry and Biochemistry, Arizona Biodesign Institute and the Center for the Study of Early Events in Photosynthesis, Arizona State University, Tempe, Arizona 85287-1604

Received: July 7, 2003; In Final Form: November 6, 2003

Energy transfer from *Rhodobacter sphaeroides* light-harvesting complex I (LHI) to the reaction center (RC) was investigated with steady-state and time-resolved fluorescence spectroscopy. Chromatophores isolated from a strain containing LHI with the mutation αTrp43 to Phe (LHI mutant) and strains containing either the LHI mutant with wild-type RCs (LHI mutant + WT RC) or the LHI mutant with the RC mutations LH(L131)+LH(M160)+FH(M197) (LHI mutant + T1 RC) were investigated at 294 and 77 K. In the LHI mutant, absorption and fluorescence spectra were blue-shifted by 21 nm compared to wild-type LHI. The energy transfer from mutated LHI to the RC occurs about two times faster than energy transfer from wild-type LHI to the RC. The acceleration of energy transfer is consistent with the increase in the energy transfer rate estimated from the spectral overlap between the RC absorbance and the LHI fluorescence according to Förster energy transfer theory.

Introduction

In photosynthetic bacteria, the light energy is captured by pigment−protein complexes called light-harvesting antenna. The purple nonsulfur bacterium *Rhodobacter (Rb.) sphaeroides* has two types of light-harvesting complexes: light-harvesting II antenna (LHII) and light-harvesting I antenna (LHI). LHII captures the light energy and rapidly transfers it to LHI, which surrounds a reaction center (RC). From LHI the excitation energy is transferred in 35−40 ps to the primary electron donor of the RC, a pair of bacteriochlorophylls (P).[1,2] In the RC, the excitation of the primary electron donor drives the electron-transfer reactions that eventually lead to the generation of the electrochemical potential gradient across the cell membrane.[3−7]

So far, only the structures of the LHII antenna and RC have been solved to atomic resolution.[8−12] The structure of the LHII complex from the purple bacterium *Rhodopseudomonas (Rps.) acidophila* was solved to 2.5 Å resolution.[8] LHII has a closed ring structure that consists of $\alpha\beta$ heterodimer protein subunits (also called $\alpha\beta$-apoprotein), which bind 27 bacteriochlorophyll (BChl) molecules. Of these, 18 BChl molecules are arranged in excitonically coupled pairs that are perpendicular to the plane of the membrane. The other 9 BChl molecules are parallel to the membrane plane. The two different sets of molecules also have distinct absorbance bands; the 9 BChl molecules parallel to the membrane plane give rise to an absorption band centered at 800 nm, while the absorption band of the 18 excitonically coupled BChl molecules is centered at 850 nm.

It is thought that the LHI antenna structure is similar to that of LHII, but a high-resolution crystal structure of the LHI or LHI + RC complex has not been published. There are still remaining questions about how LHI surrounds the RC and how many BChl molecules are associated with LHI. An electron projection map of LHI from *Rhodospirillum* (*Rs.) rubrum* was solved to 8.5-Å resolution. It was shown that LHI has a ring-like structure that has 16 $\alpha\beta$ subunits with an outer ring diameter of 116 Å and an inside hole with a diameter of roughly 68 Å.[13] The structure of LHI from *Rhodobacter (Rb.) sphaeroides* has been modeled based on sequence homology between the $\alpha\beta$-heterodimers of *Rb. sphaeroides* LHI and those of *Rhodospirillum (Rs.) molischianum* LHII[9] assuming a ring structure for LHI as found in *Rs. rubrum*. From this model, it was estimated that LHI from *Rb. sphaeroides* has 16 $\alpha\beta$-heterodimers that form a cylinder with an inside hole of 78 Å diameter and outside ring of 118 Å diameter. Having LHI as a ring and using energy minimization, the photosynthetic RC was placed into the center of the LHI ring. From this modeling it was calculated that the smallest number $\alpha\beta$-heterodimers to form a ring around the RC was 16.[14,15]

To investigate spectroscopic changes in LHI, site-directed mutagenesis was used to create mutants of the LHI antenna from *Rb. sphaeroides*. The highly conserved residue, tryptophan at position 43, of the α protein subunit (αTrp43) was changed to tyrosine (Tyr) and phenylalanine (Phe). Changing αTrp43 to Phe breaks a hydrogen bond between the protein and the C3 acetyl carbonyl group of one of the BChls in the excitonically coupled pair.[16] This gives a shift of the absorption maximum to 853 nm from the wild-type LHI absorbance peak of 875 nm. The mutation αTrp43 to Tyr forms an additional hydrogen bond to the C3 acetyl carbonyl and shifts the LHI absorption maximum to 866 nm.[16]

Previously we reported a study of energy trapping and detrapping in *Rb. sphaeroides* strains containing wild-type LHI + RC mutants with altered P/P^+ midpoint potentials.[17] In these RC mutants the initial electron-transfer rate is slowed because of an increase in the P/P^+ midpoint potential.[18] By slowing the primary electron transfer at high P/P^+ midpoint potentials (635 to 765 mV in the mutants, compared to 505 mV for wild type), energy transfer from LHI to the RC was directly observed at low temperatures (the decay of the LHI fluorescence and rise

* To whom correspondence should be addressed. Fax: (480) 965-2747. E-mail: nwoodbury@asu.edu.

10.1021/jp035956l CCC: $27.50
Published on Web 03/02/2004

in P* fluorescence were spectrally and kinetically resolved from other energy-transfer and electron-transfer processes). However, at room temperature the spectra of LHI and the RC are overlapped, interfering with direct observation of the excited state of the primary electron donor in the RC. Thus, altering some of the spectral properties of the antenna in addition to reducing the rate of the primary electron transfer in the RC may allow direct observation of the energy transfer from LHI to the RC even at room temperature. Also, changes in the spectral overlap of the LHI fluorescence and RC absorption spectra should result in changes in the energy transfer rate from the antenna to the RC as predicted by Förster energy transfer theory.

Here the energy-trapping process is investigated in membranes containing LHI with the mutation Trp to Phe at α43. These mutant LHI are examined in combination with WT reaction centers, or in combination with a triple mutant of the RC, LH(L131)+LH(M160)+FH(M197). The steady-state fluorescence and single-photon counting measurements were performed at both room and low temperatures to investigate the energy transfer from the antenna to the RC.

Materials and Methods

LHI Mutant. The LHI mutant was constructed using site-directed mutagenesis by PCR with primers designed to change αTyr43 to Phe.[16] The mutated LHI gene was subcloned into the plasmid pLH29 that contains the entire *puf* operon including the WT RC gene. Also, the mutated LHI gene was subcloned into the plasmid pRK-T1, which contains a version of the *puf* operon that includes three mutations in the RC L and M subunits, specifically, LH(L131)+LH(M160)+FH(M197) (Leu changed to His at position L131 + Leu to His at M160 + Phe to His at M197). In the subsequent descriptions, this RC mutant will be referred to as "T1" or the "triple" mutant. Both plasmids were transformed into *E. coli* S-17 and then transferred by conjugation into the deletion strain ΔBALM of *Rb. sphaeroides*.[19] Chromatophores from different strains were isolated as described previously:[17,20] LHI mutant only (no RCs), wild-type LHI in combination with wild-type RCs (referred to as wild-type LHI + WT RCs), wild-type LHI + T1 RCs, LHI mutant + WT RCs, and LHI mutant + T1 RCs. Samples were suspended in TEN buffer (50 mM Tris-HCl, pH 8.0, 1 mM EDTA, pH 8.0, and 100 mM NaCl) for room temperature measurements and in a mixture of glycerol and TEN buffer (2:1 v/v) for 77 K measurements. In addition, 10 mM sodium dithionite was added to each sample to reduce the quinone acceptors in the reaction center. For absorbance, steady-state fluorescence, and time-correlated single photon counting, an Optistat DN cryostat (Oxford Instruments) was used to cool samples to 77 K.

Absorption spectra were measured on a Cary-500 spectrophotometer (Varian). Steady-state fluorescence was measured with a home-built fluorimeter, based on SpectraPro-150 monochromators (Acton Research) and an air-cooled CCD camera (Princeton Instruments). Fluorescence spectra were measured exciting samples at 840 nm. Energy transfer was investigated by measuring fluorescence decay kinetics using time-correlated single photon counting as described previously.[17] The samples were excited with 840-nm light and fluorescence decay kinetics were measured every 10 nm from 850 to 990 nm, at 294 and 77 K. Single wavelength, high signal-to-noise emission kinetics were also measured at each temperature. At room temperature these measurements were performed at 870 nm for the LHI mutant and at 874 nm for LHI mutant + WT or T1 RCs. At lower temperatures, measurements were made at the maximum of the fluorescence spectrum of each sample and additionally at 930 nm. Data were analyzed by global fitting of the fluorescence kinetics to a sum of exponential functions convoluted with the instrument response function, using a data analysis program written locally in Matlab (Mathworks Inc).

Results

The absorption spectra of the LHI mutant only (no RCs), LHI mutant + WT RCs, LHI mutant + T1 RCs, and wild-type LHI + WT RCs samples at room temperature and 77 K are shown in Figure 1, panels a and b, respectively. At room temperature, the maximum of the wild-type LHI absorbance band is at 876 nm, while in the LHI mutant sample, the maximum of the absorbance band is blue-shifted by 21 nm to 855 nm. Absorption spectra of the LHI mutant + WT RC and the LHI mutant + T1 RC samples have three peaks in the near-IR region: one corresponds to the antenna peak at 855 nm, while the other two appear to be due to the absorption of the RC; the peaks at 805 nm and at 758 nm correspond to absorption of the RC monomer bacteriochlorophylls and bacteriopheophytins, respectively.[21−23] In the LHI mutant + WT RC sample and the LHI mutant + T1 RC sample, the heights of the 855 nm (antenna) peak and the 805 nm (RC) peak are comparable. In contrast, in the wild-type LHI + WT RC sample and the wild-type LHI + T1 RC sample (data not shown), the 876-nm antenna peak is 4−5-fold larger than the 805-nm peak of the monomer BChls in the RC (Figure 1) in absolute absorbance and more than 10-fold larger if the broad background absorbance is subtracted. Of the two samples with mutant LHI complexes, the LHI mutant + T1 RC sample shows less absorbance from the RC monomer bacteriochlorophylls and bacteriopheophytins (Bpheo) relative to the antenna absorbance than does the LHI mutant + WT RC sample at room temperature. Also, spectra of both LHI mutant + WT RC and LHI mutant + T1 RC samples are broadened on the red side of the dominant antenna absorption band (855 nm) in comparison to the LHI mutant only sample. This shoulder is due to the primary electron donor, P, of the RC.

At 77 K, the LHI mutant only near-IR absorption band has a maximum at 868 nm. This is blue-shifted by 21 nm compared to wild-type LHI, which has an absorbance maximum at 889 nm (Figure 1b). In the LHI mutant + WT RC sample, on the red side of the antenna absorption band a shoulder can be resolved near 900 nm. This shoulder can be resolved more clearly at low temperatures as the spectrum of the LHI mutant only narrows and the spectrum of the initial electron donor, P, of the RC shifts to about 890 nm.[21,22] As is observed in isolated RCs at 77 K, the RC Bpheo molecules have an absorbance peak at 759 nm and the monomer bacteriochlorophylls absorb at 805 nm.

In the LHI mutant + T1 RC sample at 77 K, one can also resolve the absorbance band of P, but not as well as in the LHI mutant + WT RC sample, most likely because the P band is less intense in the T1 RC mutant at low temperature than it is in WT RCs. Similar to what was observed in the room temperature absorption spectra, the intensities of the RC monomer BChl and Bpheo absorption bands in the LHI mutant + T1 RC sample are lower, relative to the antenna band, than in the LHI mutant + WT RC sample. However, in the T1 RC mutant at 77 K, two bands at 800 and 811 nm, which probably correspond to B_A and B_B molecules, respectively, can be resolved.[3] In the LHI mutant + T1 RC sample, the RC Bpheo peak is at 759 nm and again is less intense compared with the LHI mutant + WT RC sample.

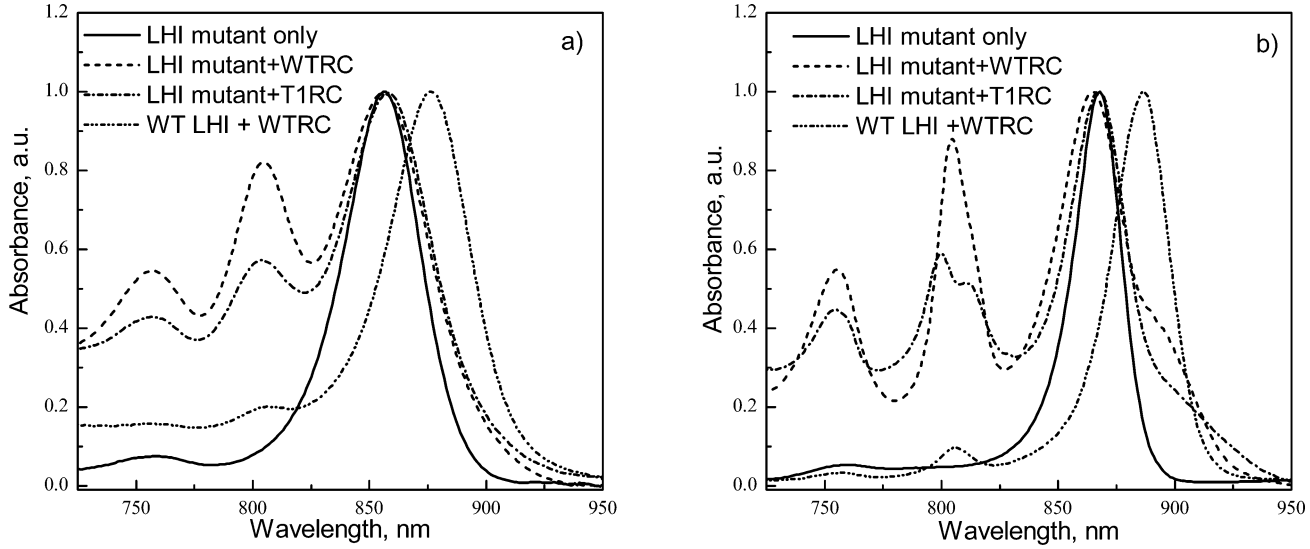

Figure 1. Ground state absorption spectra at room temperature (a) and 77 K (b). LHI mutant only sample (solid line), LHI mutant + WT RC sample (dashed line), and LHI mutant + T1 RC sample (dash-dot line) and wild-type LHI + WT RC sample (dash-dot-dot line). Spectra were normalized at the maximum of the antenna band at 857 nm at room temperature and 868 nm at 77 K for mutant antenna and at the absorbance maximum of wild-type LHI.

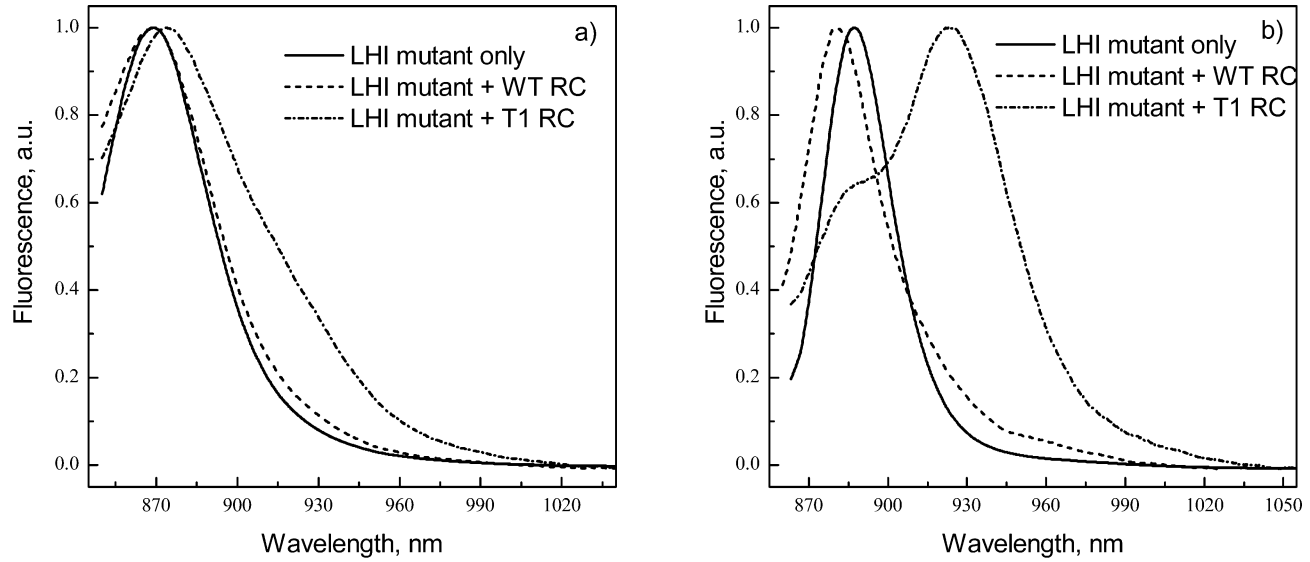

Figure 2. Steady state fluorescence at room temperature (a) and 77 K (b). LHI mutant only sample (solid line), LHI mutant + WT RC sample (dashed line), and LHI mutant + T1 RC sample (dash-dot line). Spectra were normalized at their maxima.

Steady-state fluorescence spectra measured at room temperature and 77 K are shown in Figure 2. As seen for the absorption spectrum at room temperature, the fluorescence spectrum of the LHI mutant is blue-shifted by 21 nm compared to the wild-type LHI spectrum (the maximum for the LHI mutant is at 869 nm and that for the wild-type LHI is at 890 nm).[24] The fluorescence spectrum of the LHI mutant + WT RC sample has a maximum at 870 nm and a slightly increased intensity on the red side of the spectrum in the 900−960 nm region, compared with the LHI mutant only. The increase in red side fluorescence in the mutant is most likely due to RC emission from P. The LHI mutant + T1 RC sample has a fluorescence maximum at 873 nm, a 4 nm red shift compared to the LHI mutant only, and a higher intensity red shoulder presumably due to fluorescence from the RC, which has an emission peak near 910−920 nm.

At 77 K, the fluorescence spectrum of the LHI mutant has a maximum at 887 nm (see Figure 2b), which is again blue-shifted by 21 nm compared to wild-type LHI. The most interesting result of the 77 K steady state fluorescence measurements is that in the LHI mutant + T1 RC sample, the spectrum has two clearly resolved peaks. Surprisingly, the antenna fluorescence at 887 nm is less intense than the 923 nm fluorescence peak, which is due to the T1 RCs. Apparently, the yield of fluorescence from P* in the T1 RCs is higher than that from the excited state of the mutated antenna. This result will be discussed below in terms of the kinetics of energy and electron transfer. The LHI mutant + WT RC sample has a fluorescence maximum at 880 nm at 77 K, which is blue-shifted relative to the spectrum of the LHI mutant. The fluorescence spectrum also contains a small red shoulder between 910 and 990 nm, due to fluorescence from the WT RC.

Energy transfer from LHI to the RC in the mutants was investigated by time-correlated single-photon counting. High signal-to-noise ratio kinetic measurements were performed at the fluorescence maximum of each sample, and the results were fitted to the minimum required number of exponential decay functions (Figure 3). In addition, sets of fluorescence kinetics for each sample, at both room temperature and 77 K, were measured every 10 nm covering the whole fluorescence spectra.

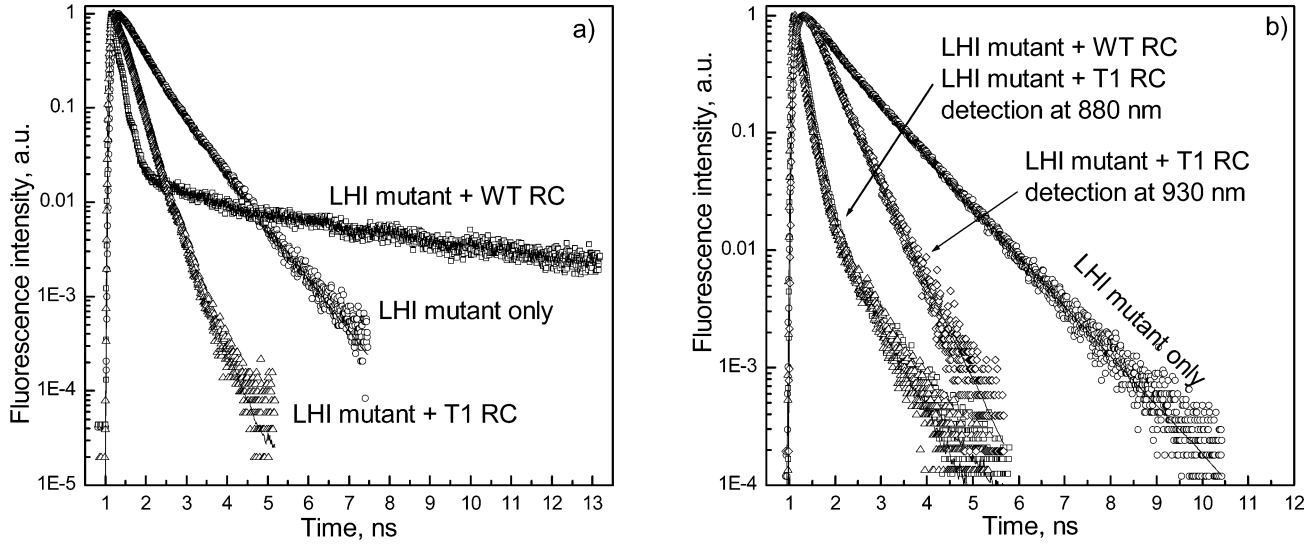

Figure 3. Fluorescence kinetics at room temperature (a) and 77 K (b). In both panels a and b the excitation is at 840 nm and emission detection at 880 nm. The LHI mutant only sample fluorescence kinetics are shown as open circles and the fit is shown as a solid line, and the LHI mutant + WT RC sample fluorescence kinetics are shown as open squares and the fit as a solid line. For the LHI mutant + T1 RC sample, excitation is at 840 nm and emission is collection at 880 and 930 nm. Time decays are shown as open triangles (880 nm emission) and open diamonds (930 nm emission) and the fits as solid lines. Fluorescence kinetics are normalized to 1 at their respective maxima.

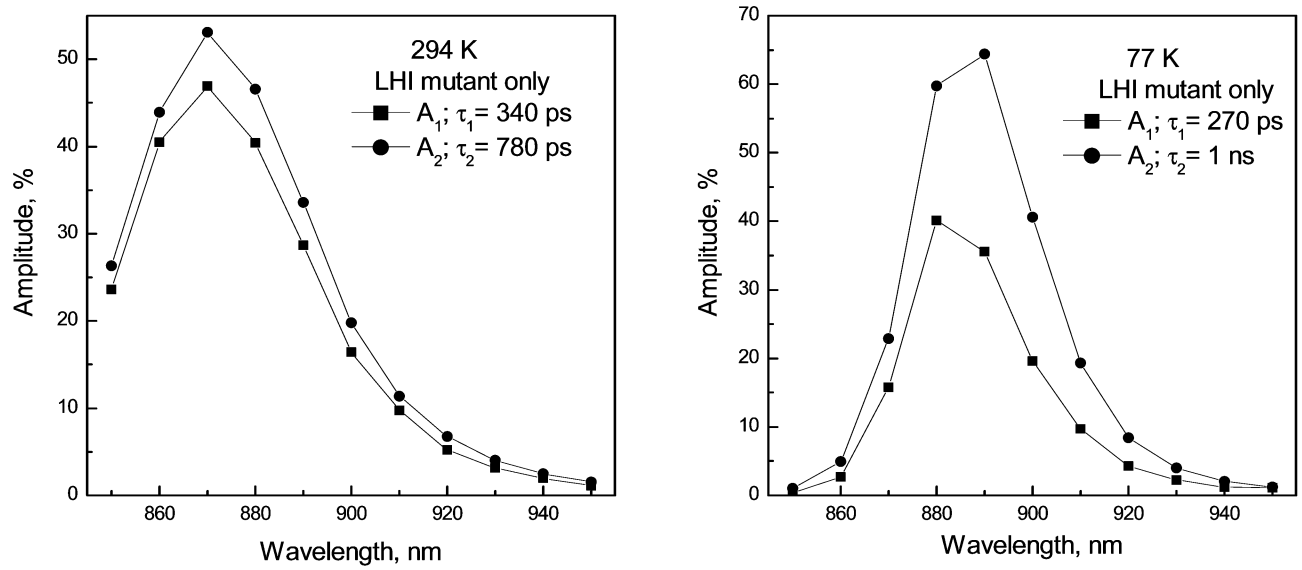

Figure 4. Decay-associated spectra resulting from fits of the fluorescence decays from chromatophores containing the LHI mutant only (no RCs), at 294 and 77 K.

Decay associated spectra (DAS) were constructed from global fits of these fluorescence kinetics (see Figures 4−6).

Kinetics of the LHI mutant only fluorescence decay were fitted with two-exponential decay (see Figure 3 for kinetics and Figure 4 for DAS). The first component's lifetime was 340 ps at room temperature and the relative amplitude was about 45%. The second component's lifetime was 780 ps and the amplitude was about 55% at room temperature. At 77 K, the first component decayed faster, with a lifetime of 270 ps, and the second component decayed slower than at room temperature, with a lifetime of 1 ns. The faster component amplitude decreased to 40% and the slower component amplitude increased to 60% at 77 K compared with room temperature values.

The initial fluorescence (up to 2 ns) for the LHI mutant + WT RC sample decays much faster than does the fluorescence from the LHI mutant only sample (see Figure 3). However, it also contains a very slowly decaying fraction that most likely represents delayed fluorescence (see below). The fluorescence kinetics for the LHI mutant + WT RC sample had to be fitted with a four-exponential decay at room temperature (see Figure 5 for DAS). The major (about 87%) component has a decay lifetime of 20 ps and is due to the quenching of the antenna fluorescence by the RC. The second component has a lifetime of 57 ps, the third component decays in 950 ps, and the last component lives for 7 ns. The longest three components have much smaller amplitudes and are thought to represent the equilibration between the excited states of LHI and P and the charge-separated state $P^+H_A^-$.[25,17]

At 77 K, the fluorescence decay kinetics of the LHI mutant + WT RC sample were still significantly faster than the fluorescence decay of the LHI mutant only sample. However, at low temperatures the longest lived component of the fluorescence decay from the RC-containing sample disappeared. The fluorescence kinetics, therefore, were fitted with only three-exponential decays. The first component still had a lifetime of 20 ps, and again represented the quenching of the antenna

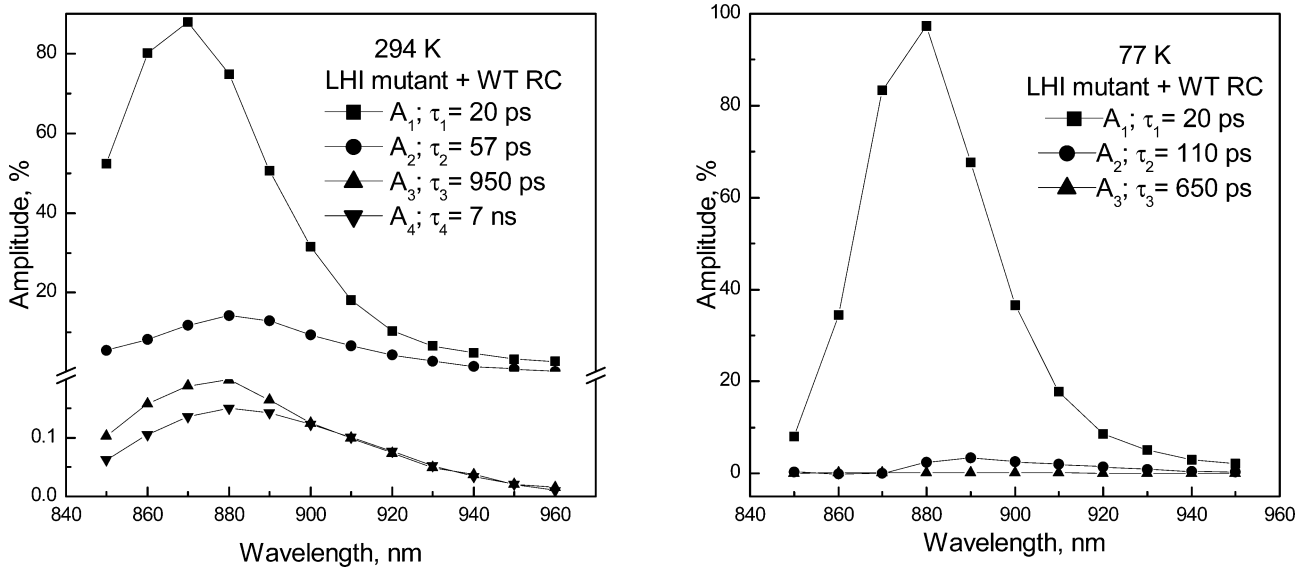

Figure 5. Decay-associated spectra resulting from fits of the fluorescence decay from chromatophores containing the LH I mutant + WT RC, at 294 and 77 K. Notice the break of the amplitude axis in the room temperature results.

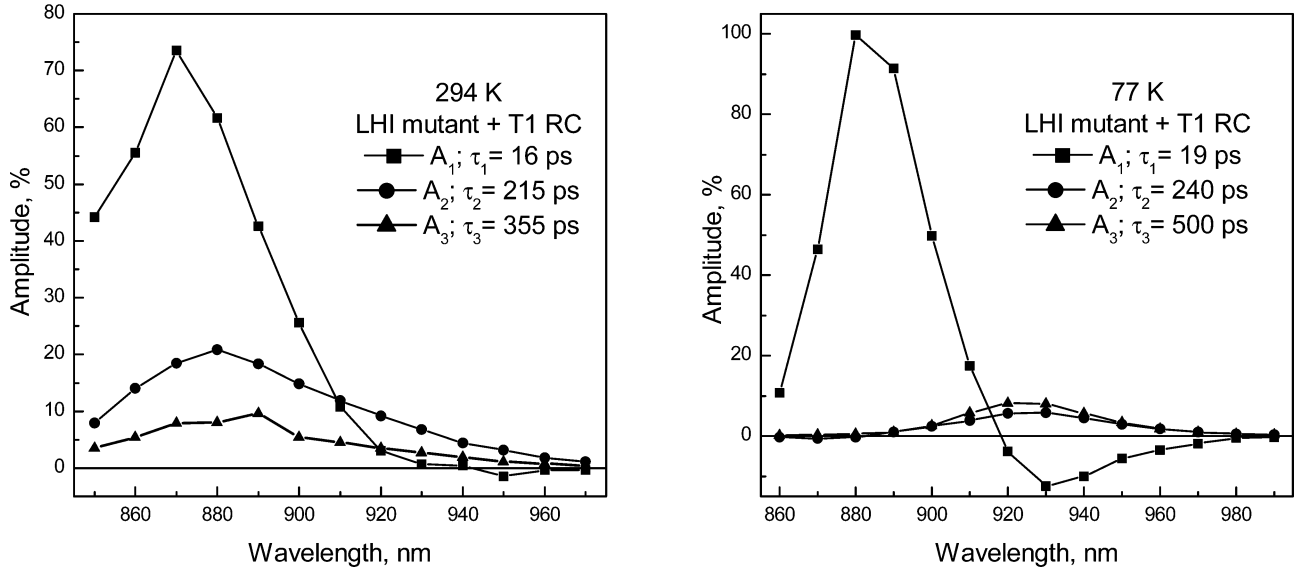

Figure 6. Decay-associated spectra resulting from fits of the fluorescent decay from chromatophores containing the LH I mutant with T1 (LH-(L131)+LH(M160)+FH(M197)) mutant reaction centers (P/P^+ midpoint potential of 765 mV), at 294 and 77 K.

fluorescence by the RC (see Figure 5 for DAS). The second component was slower at 77 K than at room temperature, decaying with the lifetime of 110 ps, while the final component was faster and decayed in 650 ps. Interestingly, the spectrum of the second component (110 ps) at 77 K had a small dip to negative amplitudes around 860 nm, and a red-shifted maximum at around 890 nm compared to the maximum of the 20-ps component at 880 nm (see Figure S1 in the Supporting Information). The spectral shift of the second component is consistent with energy equilibration occurring between the excited LHI antennas and the excited/charge-separated states of the RC.

In the case of the LHI mutant + T1 RC sample, the fluorescence kinetics decayed faster than in the LHI mutant only, showing that there is energy trapping from the antenna to the RC (see Figure 3). Additionally, the longest lived component observed in the LHI mutant + WT RC sample was not found in the LHI mutant + T1 RC sample. At 77 K, the fluorescence decay kinetics changed with emission wavelength dramatically: at 880 nm, the fluorescence decay is very similar to the LHI mutant + WT RC sample, but at 930 nm, much slower decay kinetics can be resolved (Figure 3b). The fluorescence decays were fitted with three-exponential components at both 294 and 77 K. The DAS for the LHI mutant + T1 RC sample are shown in Figure 6. At 294 K, the first component has a lifetime of 16 ps and an amplitude of about 72% at the maximum emission wavelength (880 nm). Notice that this component has a negative amplitude between 950 and 970 nm showing that the energy transfer from the antenna to the RC can be resolved even at room temperature. The second component decays in 215 ps, and the third in 355 ps. At 77 K in the LHI mutant + T1 RC sample, the first component decays with a lifetime of 19 ps and comprises almost 100% of the amplitude at the emission maximum of 880 nm. However, the amplitude spectrum of this component is negative from 920 to 970 nm, representing energy transfer occurring from the antenna to the RC. The second component has a lifetime of 240 ps and a maximum amplitude at 920 nm, corresponding to fluorescence from the RC. As observed for the LHI mutant + WT RC sample, the 240-ps component has a small negative amplitude

from 860 to 880 nm (see Figure S2 in the Supporting Information). The last component decayed with a lifetime of 500 ps and has maximum emission amplitude at 920 nm, again due to fluorescence from the RC.

Discussion

Previously we have reported that energy transfer from the excited state of LHI to the initial electron donor P could be directly observed in the high P/P^+ midpoint potential RC mutants LH(L131)+LH(M160)+LHI and LH(L131)+LH-(M160)+FH(M197)+LHI (referred to here as T1) at cryogenic temperatures.[17] In these mutants, the P/P^+ midpoint potential is increased relative to the WT RC by 160 and 260 mV, respectively. The free energy of the state $P^+H_A^-$ is shifted toward P^* by approximately the same amount, making P* and $P^+H_A^-$ almost isoenergetic in the triple mutant.[26] The change in energetics is reflected in the primary electron-transfer time constant, which slows down from 3.5 ps in WT to 52 ps in the triple mutant RCs at room temperature.[25,26] The decrease in the electron-transfer rate constant results in a significant increase in the P* fluorescence quantum yield, thus making it possible to observe the fluorescence from P* as the energy is transferred from LHI. However, the spectral overlap of the fluorescence from the LHI antenna and P hinders the resolution of the two states, especially at room temperature. Therefore, energy transfer from a mutated LHI that is better resolved spectrally from the RC was investigated. As described above, the mutation Trp 43 to Phe in the α subunit of LHI results in a blue-shift of the absorbance and fluorescence spectra by 21 nm.[16] This should allow better spectral resolution of LHI and P fluorescence.

As expected, the larger separation of the fluorescence bands in the LHI mutant + T1 RC sample resulted in the ability to directly observe the energy-transfer process from the mutated antenna to the RC, even at room temperature (see Figure 6). This was not observed in the wild-type LHI + T1 RC sample. In fact, the mutated LHI also provided better kinetic resolution of P* decay as well. The LHI mutation results in a 2-fold increase in the rate of energy transfer between LHI and the RC (see below). This coupled with the fact that P* decays much more slowly in T1 RCs relative to wild-type RCs at room temperature (52 ps vs 3 ps)[26] resulted in a higher intermediate population of P* at any given time. Because of these spectral and kinetic changes, the decay of the LHI excited state and rise of P* fluorescence manifests itself in the spectrum of the fastest fluorescence decay component in Figure 6 as a change in amplitude from positive values below 930 nm (decay of the antenna fluorescence) to negative values between 930 and 960 nm (rise of fluorescence from P*).

At 77 K in the LHI mutant + T1 RC, the spectral features associated with antenna to RC energy transfer are even more clearly apparent. The decay-associated spectrum of the fastest fluorescence decay component (19 ps) changes from positive values below 910 nm to negative values between 920 and 970 nm (see Figure 6). The second and third components, with lifetimes of 240 and 500 ps, both have maximum amplitudes at 920 nm and can be attributed to fluorescence from P*.[7] This is in contrast to the situation at room temperature where the antenna fluorescence dominates the decay-associated spectrum of the second decay component presumably due to energy equilibration between the excited states of RC and LHI favoring the antenna (Figure 6). The second and third decay component's overall kinetics and fluorescence spectra at low temperature probably represent equilibration between P* and $P^+H_A^-$, followed by relaxation and decay of the charge-separated state.[25]

Unfortunately, the improved spectral resolution afforded by the LHI mutant with WT RCs does not allow the direct observation of the rise in P* fluorescence during energy transfer in the LHI mutant + WT RC sample. In WT RCs, the P* fluorescence yield is very low because the primary electron-transfer rate is more than 5-fold faster than the rate of energy transfer from LHI to the RC; thus the rise of P* fluorescence at 920 nm cannot be resolved (see Figure 5). However, in the LHI mutant + WT RC sample, as was true in the LHI mutant + T1 RC sample, the energy trapping from the mutated antenna to the RC occurs about two-times faster than observed in wild-type LHI +WT RC (20 and 42 ps, respectively).[17] The second fluorescence decay component in the LHI mutant + WT RC sample at room temperature also decays severalfold faster than in wild-type LHI + WT RC, 57 and 200 ps, respectively. On the other hand, the lifetimes of the longest two fluorescence decay components are slightly slower in the LHI mutant + WT RC sample than in the wild-type LHI + WT RC sample (950 ps in the LHI mutant vs 740 ps in wild type for the third component and 7 ns for the LHI mutant vs 6.5 ns in wild type for the fourth component).

At 77 K, the same trends in the results are observed; the lifetime of the first decay component is faster in the LHI mutant + WT RC sample compared to the wild-type LHI + WT RC sample. It should also be noted that in the LHI mutant + WT RC sample at 77 K, the nanosecond component is not resolved. This most likely arises because the energy of the excited mutant antenna is higher than that of the wild type, making equilibration with the charge-separated state less favorable, particularly at low temperature.

The changes in the trapping rate constant between wild-type LHI and the LHI mutant-containing samples can be discussed in terms of Förster energy transfer theory. Previously, several theoretical studies on energy transfer both within the antenna and between the antenna and the RC have concluded that the trapping step can be adequately described using a Förster mechanism.[1,24,27−33] In this theory, the energy-transfer rate depends on several factors: the relative arrangement of the donor and acceptor molecules, the distance between them, the fluorescence lifetime, and the quantum yield of the donor, as well as the spectral overlap between donor fluorescence and acceptor absorbance transitions.[34] Our results show that the trapping in samples containing the LHI mutant is nearly 2-fold faster than that in samples containing wild-type LHI. There is no obvious reason to think that major changes in distance and orientation have occurred in the mutant studied here. However, the spectral overlap between the mutant antenna fluorescence and the RC (P) absorbance spectra is clearly increased (Figure 7). The LHI mutant fluorescence is shifted by 21 nm to the blue (maximum at 869 nm at room temperature), and it much better overlaps the absorbance of the P band of the RC (maximum at 868 nm). The spectral overlap between the fluorescence from the LHI mutant antenna and RC absorbance at room temperature was calculated to be about 1.6-fold larger than the overlap between the wild-type LHI fluorescence spectrum and the RC absorbance spectrum and 2.3-fold larger at 77 K. This is consistent with the roughly 2-fold increase in energy-transfer rate between the mutant LHI antenna and the RC relative to wild-type LHI. As might be expected for a rate change due to spectral overlap, roughly the same increase in rate is observed at both room temperature and 77 K, and for transfer either to WT RCs or T1 RCs.

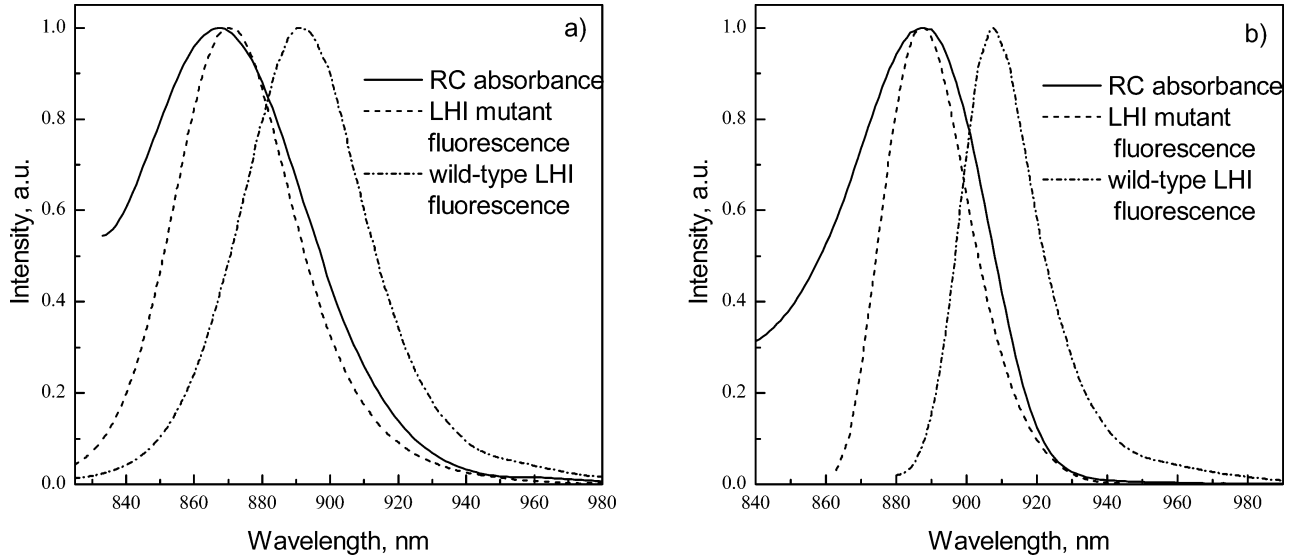

Figure 7. The spectral overlap between RC absorbance and antenna fluorescence at room temperature (a) and 77 K (b).

One of the most obvious differences between wild-type LHI and the mutant described here is that the reaction center absorbance transitions are much more prominent in the spectrum of the mutant than in the wild type (Figure 1). Clearly, the reaction centers are assembling with the mutant LHI antenna, as evidenced by the very rapid energy transfer between these components. However, the structural arrangement of the LHI mutant/RC complex is not clear. Analysis of the ground-state absorption spectra and steady-state fluorescence spectra of the LHI mutant antenna shows that the number of bacteriochlorophyll molecules in the antenna is decreased relative to wild type. Previously it was estimated that in wild-type LHI there are 32 bacteriochlorophylls.[14,35] In contrast, calculations based on the absorbance spectrum of the LHI mutant + WT RC sample show that there are at least 5 times fewer BChl per RC than in the wild-type LHI +WT RC sample (comparing the relative size of the monomer BChl band of the RC to the LHI antenna absorbance).

On the basis of results described above, one could speculate that the Tyr to Phe mutation in the α subunit of LHI interrupts the assembly process in the antenna, resulting in incomplete rings. Previously it has been shown that other factors, such as the *PufX* gene product, can determine the structure and BChl content of LHI. In *Rb. sphaeroides* lacking the *PufX* gene, LHI has a closed ring structure with about 15−17 $\alpha\beta$-subunits and 30−34 BChl molecules per RC.[35] However, in *Rb. sphaeroides* containing the *PufX* gene, LHI + RC complexes consisted of two open C-shaped rings (12 $\alpha\beta$-subunits and 24−25 BChl each), each containing a RC.[36,37]

Of course an alternative explanation for the low BChl to RC ratio is that the system is radically heterogeneous and a small number of RC/antenna complexes assemble normally, while most RCs remain in the membrane without antenna. There is no reason to think the LHI mutation studied here would give rise to such a heterogeneous system, but it remains a formal possibility. However, this does not substantially change the conclusions regarding energy transfer, which can only take place in complexes that contain both antenna and reaction centers.

Acknowledgment. This research was supported by USDA grant 2001-35318-10931 and NSF grant MCB-0131764. This is publication No. 585 from the Center for the Study of Early Events in Photosynthesis at Arizona State University.

Supporting Information Available: Enlargements of decay-associated spectra in FIgures 5 and 6. This material is available free of charge via the Internet at http://pubs.acs.org.

References and Notes

(1) van Amerongen, H.; Valkunas, L.; van Grondelle, R. *Photosynthetic excitons*; World Scientific Publishing Co.: Singapore, 2000.

(2) Freiberg, A. Coupling of antennas to reaction centers. In *Anoxygenic Photosynthetic Bacteria*; Blankenship, R. E., Madigan, M. T., Bauer, C. E., Eds.; Kluwer Academic Publishers: Dordrecht, Thge Netherlands, 1995; Vol. 2, pp 385−398.

(3) Hoff, H. J.; Deisenhofer, J. *Phys. Rep.* **1997**, *287*, 1−247.

(4) Kirmaier, C.; Holten, D. Electron transfer and charge recombination reactions in wild-type and mutant bacterial reaction centers. In *The Photosynthetic Reaction Center*; Deisenhofer, J., Norris, J. R., Eds.; Academic Press: San Diego, CA, 1993; Vol. II, pp 49−70.

(5) Kirmaier, C.; Holten, D. *Photosynth. Res.* **1987**, *13*, 225−260.

(6) Parson, W. W. Photosynthetic bacterial reaction centres. In *Protein Electron Transfer*; Bendall, S. D., Ed.; BIOS Scientific Publishers: Oxford, UK, 1996; pp 125−160.

(7) Woodbury, N. W.; Allen, J. P. The pathway, kinetics and thermodynamics of electron transfer in wild type and mutant reaction centers of purple nonsulfur bacteria. In *Anoxygenic Photosynthetic Bacteria*; Blankenship, R. E., Madigan, M. T., Bauer, C. E., Eds.; Kluwer Academic Publishers: Dordrecht, The Netherlands, 1995; Vol. 2, pp 527−557.

(8) McDermott, G.; Prince, S. M.; Freer, A. A.; Hawthornthwaite-Lawless, A. M.; Papiz, M. Z.; Cogdell, R. J.; Isaacs, N. W. *Nature* **1995**, *374*, 517−521.

(9) Koepke, J.; Hu, X.; Munke, K.; Schulten, K.; Michel, H. *Structure* **1996**, *4*, 581−597.

(10) Deisenhofer, J.; Epp, O.; Miki, K.; Huber, R.; Michel, H. *J. Mol. Biol.* **1984**, *180*, 385−398.

(11) Deisenhofer, J.; Epp, O.; Miki, K.; Huber, R.; Michel, H. *Nature* **1985**, *318*, 618−624.

(12) Allen, J. P.; Feher, G.; Yeates, T. O.; Komiya, H.; Rees, D. C. *Proc. Natl. Acad. Sci. U.S.A.* **1987**, *84*, 5730−5734.

(13) Karrasch, S.; Bullough, P. A.; Ghosh, R. *EMBO J.* **1995**, *14*, 631−638.

(14) Hu, X.; Schulten, K. *Biophys. J.* **1998**, *75*, 683−694.

(15) Hu, X.; Damjanovic, A.; Ritz, T.; Schulten, K. *Proc. Natl. Acad. Sci. U.S.A.* **1998**, *95*, 5935−5941.

(16) Olsen, J. D.; Sockalingum, G. D.; Robert, B.; Hunter, C. N. *Proc. Natl. Acad. Sci. U.S.A.* **1994**, *91*, 7124−7128.

(17) Katiliene, Z.; Katilius, E.; Woodbury, W. N. *Biophys. J.* **2003**, *84*, 3240−3251.

(18) Allen, J. P.; Williams, J. C. *J. Bioenerg. Biomembr.* **1995**, *27*, 275−283.

(19) Williams, J. C.; Taguchi, A. K. W. Genetic manipulations of purple photosynthetic bacteria. In *Anoxygenic Photosynthetic Bacteria*; Blankenship, R. E., Madigan, M. T., Bauer, C. E., Eds.; Kluwer Academic Publishers: Dordrecht, The Netherlands, 1995; Vol. 2, pp 1029−1065.

(20) Freiberg, A.; Allen, J. P.; Williams, J. C.; Woodbury, N. W. *Photosynth. Res.* **1996**, *48*, 309−319.

(21) Katilius, E.; Katiliene, Z.; Lin, S.; Taguchi, A. K. W.; Woodbury, N. W. *J. Phys. Chem. B* **2002**, *106*, 1471−1475.
(22) van Brederode, M. E. New pathways for ultrafast electron transfer in photosynthetic reaction centers of *Rhodobacter sphaeroides*, Free University of Amsterdam, 1999.
(23) van Brederode, M. E.; Jones, M. R. *Subcell. Biochem.* **2000**, *35*, 621−676.
(24) Hess, S.; Visscher, K. J.; Ulander, J.; Pullerits, T.; Jones, M. R.; Hunter, C. N.; Sundstrom, V. *Biochemistry* **1993**, *32*, 10314−10322.
(25) Peloquin, J. M.; Williams, J. C.; Lin, X.; Alden, R. G.; Taguchi, A. K. W.; Allen, J. P.; Woodbury, N. W. *Biochemistry* **1994**, *33*, 8089−8100.
(26) Woodbury, N. W.; Lin, S.; Lin, X.; Peloquin, J. M.; Taguchi, A. K. W.; Williams, J. C.; Allen, J. P. *Chem. Phys.* **1995**, *197*, 405−421.
(27) Pearlstein, R. *Photochem. Photobiol.* **1982**, *35*, 835−844.
(28) Damjanovic, A.; Ritz, T.; Schulten, K. *Int. J. Quantum Chem.* **2000**, *77*, 139−151.
(29) van Grondelle, R. *Biochim. Biophys. Acta* **1985**, *811*, 147−195.
(30) Freiberg, A.; Godik, V.; Pullerits, T.; Timpmann, K. *Biochim. Biophys. Acta* **1989**, *973*, 93−104.
(31) Zhang, F. G.; Gillbro, T.; van Grondelle, R.; Sundstrom, V. *Biophys. J.* **1992**, *61*, 694−703.
(32) Bergstrom, H.; van Grondelle, R.; Sundstrom, V. *FEBS Lett.* **1989**, *250*, 503−508.
(33) Visscher, K. J.; Bergstrom, H.; Sundstrom, V.; Hunter, C. N.; van Grondelle, R. *Photosynth. Res.* **1989**, 211−217.
(34) Lakowicz, J. R. *Principles of fluorescence spectroscopy*, 2nd ed.; Kluwer Academic/Plenum: New York, 1999.
(35) Walz, T.; Jamieson, S. J.; Bowers, C. M.; Bullough, P. A. *J. Mol. Biol.* **1998**, *282*, 833−845.
(36) Jungas, C.; Ranck, J. L.; Rigaud, J. L.; Joliot, P.; Vermeglio, A. *EMBO J.* **1999**, *18*, 534−542.
(37) Vermeglio, A.; Joliot, P. *Biochim. Biophys. Acta* **2002**, *1555*, 60−64.